 ISBN: 978-1-926872-32-2

APPLICABILITY OF NEAR-INFRARED HYPERSPECTRAL IMAGERY (NIR-HI) FOR SENSOR BASED SORTING OF AN EPITHERMAL AU-AG ORE

*M. Dalm[1], M.W.N. Buxton[1], F.J.A. van Ruitenbeek[2]

[1]Delft University of Technology
Faculty of Civil Engineering and Geosciences, Resource Engineering Section
Stevinweg 1, 2600 GA, Delft, The Netherlands
*(*corresponding author: m.dalm@tudelft.nl)*

[2]University of Twente
Faculty of Geo-Information Science and Earth Observation (ITC), Department of Earth Systems Analysis
Hengelosestraat 99, 7500 AA, Enschede, The Netherlands

ABSTRACT

In the presented study test work was performed with near-infrared hyperspectral imagery (NIR-HI) on 36 ore samples from a South-American epithermal Au-Ag mine. The aim of the test work was to investigate if NIR-HI provides information about the alteration mineralogy of samples that can be used to predict their economic value. Mineral distribution maps were produced from the hyperspectral images by using correlation coefficients between the image pixels and a set of reference spectra. These maps showed that detection of mineralogy with NIR-HI can be used to distinguish; i) ore particles with low Au and Ag grades, ii) ore particles with high carbon contents, iii) ore particles with high sulphur contents.

KEYWORDS

Sensor based sorting, Ore sorting, near-infrared, NIR hyperspectral imagery, Epithermal Au-Ag

 ISBN: 978-1-926872-32-2

INTRODUCTION

Sensor based sorting represents all applications in which singular particles are measured by a sensor and mechanically separated by using a classification based on certain physical and/or chemical properties. The technique has potential to be used as a pre-concentration step in mineral processing operations to eliminate waste and sub-economic ore prior to conventional treatment. It could therefore reduce the costs associated with processing mined materials (Salter & Wyatt, 1991; Sivamohan & Forssberg, 1991; Wotruba & Riedel, 2005; Dalm, Buxton, van Ruitenbeek, & Voncken, 2014; Buxton & Benndorf, 2013a; Buxton & Benndorf, 2013b).

Application of sensor based sorting in mineral processing requires real-time sensors that detect physical and/or chemical parameters that indicate the economic value of individual rock particles. No real-time sensors or combinations of sensors are currently known that can directly detect the Au and Ag contents of epithermal Au-Ag ores. However, the deposition of Au and Ag at epithermal deposits is accompanied by the co-deposition of certain alteration minerals (Pirajno, 1992; Simmons, White, & John, 2005). These alteration minerals can often be detected with near-infrared (NIR) spectral sensors (Thompson, Hauff, & Robitaille, 1999; AusSpec, 2008).

Near-infrared hyperspectral imagery (NIR-HI) is a sensor technique that is used to capture images of objects at many different wavelengths in the NIR spectral range. Each pixel in the resulting image represents a spectrum that contains the intensity of reflected NIR radiation as a function of wavelength. Wavelengths that are commonly recorded with NIR-HI range from 450 to 2500 nm. Certain solid materials absorb radiation around specific wavelengths in this region. This is caused by electronic molecular processes and/or molecule bond vibrations (Hunt, 1977; Clark, 1999). NIR spectroscopy can be used to identify minerals by analysing the locations, shapes and relative intensities of all absorption features in a NIR spectrum. Not all minerals can be identified with NIR spectroscopy. It is restricted to minerals containing elements or molecule bonds that produce diagnostic absorptions. Minerals that produce diagnostic absorptions are referred to as NIR active minerals.

SENSOR BASED SORTING

Figure 1 presents an example of the working principle of sensor based sorting. The numbers in this figure refer to the different sub-processes into which sensor based sorting is generally subdivided (Salter & Wyatt, 1991; Wotruba & Riedel, 2005). These sub-processes are the following:

1) Particle presentation
2) Particle examination
3) Data processing
4) Particle separation

The aim of particle presentation in sensor based sorting is to redistribute the incoming material in such a way that individual particles do not touch each other. This is necessary to allow examination and separation of every individual particle. Particle presentation is usually achieved by accelerating the incoming material. In the example in figure 1, this is performed by transferring the material onto a faster moving conveyor belt. Another common method for particle presentation is by using a chute (Wotruba & Riedel, 2005; Harbeck & Kroog, 2008).

Examination of the individual particles is performed by using one or more sensors. Sensor types that can be used for sensor based sorting include optical, near-infrared, X-ray transmission, X-ray fluorescence and electromagnetic sensors (Harbeck & Kroog, 2008; Bergmann, 2011). After particle examination, the recorded sensor data is processed by a computer. The computer makes a decision on how to classify a certain particle and sends a signal to the particle separation unit. Particle separation is usually performed by using jets of compressed air (Wotruba & Riedel, 2005).

 ISBN: 978-1-926872-32-2

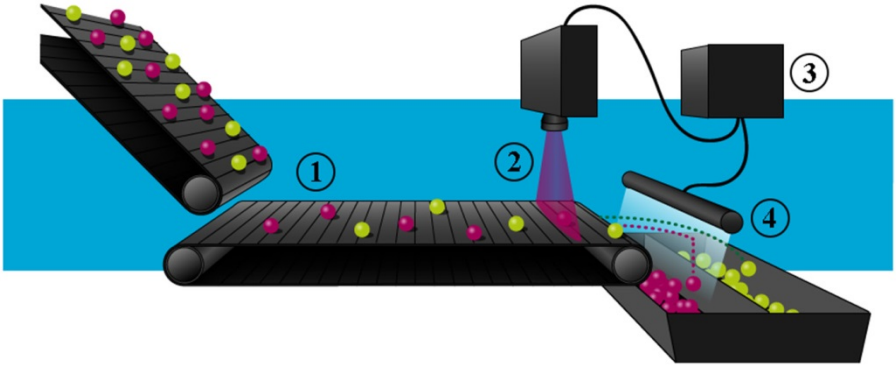

Figure 1 - Working principle of sensor based sorting

HYDROTHERMAL ALTERATION AT EPITHERMAL ORE DEPOSITS

Epithermal Au-Ag deposits are formed by hydrothermal activity that is driven by a magmatic intrusion occurring at several kilometres below the Earth's surface. Hydrothermal activity is the movement of hot aqueous (hydrothermal) fluids through the Earth's crust and interaction between these fluids and the rocks through which they pass. The hydrothermal fluids responsible for epithermal deposit formation originate from the magma and are released due to cooling of the magmatic intrusion (Pirajno, 1992). Au, Ag and other elements are dissolved within these fluids as ions or complex ions. After release from the magma, the hydrothermal fluids flow towards the surface due to the relatively high pressure and temperature. The ascending magmatic fluids may subsequently mix with meteoric fluids which changes the fluid chemistry and temperature.

Epithermal Au-Ag deposits form at depths up to 1500 m below the surface and temperatures < 300 °C. Sharp pressure and temperature gradients in this environment result in boiling of the hydrothermal fluids, which changes fluid composition and forces Au and Ag to precipitate (Simmons, White, & John, 2005; Pirajno, 1992). The hydrothermal fluids that introduce Au and Ag in epithermal deposits also introduce, remove and/or redistribute other pre-existing components of the host rock. This is referred to as hydrothermal alteration (Pirajno, 1992). Hydrothermal alteration results in the formation of alteration minerals. The type of alteration minerals that are formed depends on the pressure and temperature of the hydrothermal fluids and on the composition of both the hydrothermal fluids and the host rock (Pirajno, 1992). Because precipitation of Au and Ag also depends on hydrothermal fluid properties, it is related to the formation of specific alteration minerals (Simmons, White, & John, 2005; Sillitoe, 1993; White & Hedenquist, 1995).

SORTING OBJECTIVES OF THE TEST WORK

Test work was performed to investigate the applicability of NIR-HI to characterise epithermal Au-Ag ores in terms of economic value. The economic value of the ore samples that were used for the testwork mainly depends on the Au grade. Ag is mined as a by-product and higher Ag grades increase ore value. Relatively high concentrations of carbonaceous materials or sulphide minerals on the other hand decrease ore value because these lower the recovery of Au and Ag during ore processing. The objectives of the testwork were therefore to investigate if an NIR sensor can be used to distinguish; i) ore particles with low Au and Ag grades, ii) ore particles with high carbon contents, iii) ore particles with high sulphur contents.

 ISBN: 978-1-926872-32-2

METHODS

Test work approach

The test work included NIR-HI on 36 samples that originate from a South-American mine. This mine exploits a high-sulphidation epithermal Au-Ag deposit. Each sample is a rock particle of about 5-15 cm in diameter. The samples were selected at random from around the same location in the mine. Figure 2 presents a photo of the samples that were used in the testwork.

NIR hyperspectral images of the samples were acquired with a Corescan Hyperspectral Core Imager 3 (HCI-3). This device records hyperspectral images on 514 spectral bands at wavelengths ranging from 450 to 2500 nm. The pixel size of the images is about 0.5 x 0.5 mm.

By using the SIMPLISMA method (Windig & Guilment, 1991), the purest pixel spectra were extracted from the NIR hyperspectral images. The NIR active mineralogy was determined from these pure spectra by comparing the spectra with those from the G-MEX spectral interpretation field manual (AusSpec, 2008) and the USGS spectral library (Clark, et al., 2007). Subsequently, a list of mineral reference spectra was selected from the pure spectra. The pixels of the NIR hyperspectral images were classified on mineralogy by using correlation coefficients between the pixel spectra and the list of reference spectra. This classification was used to create mineral distribution maps. The mineral distribution maps were checked manually and the spectra of misclassified pixels were added to the list of reference spectra. The classification of pixel spectra was then performed again to produce new mineral distribution maps. This was carried out in an iterative manner until no more misclassified pixels were observed.

After acquiring the NIR hyperspectral images all the samples were pulverized to produce powders. X-ray diffraction (XRD) was performed on these powders to validate the NIR active mineralogy that was determined from the NIR hyperspectral images. Furthermore, fire assay was performed on the powders to determine the Au and Ag grades of samples. Finally, a LECO analyser was used to determine the carbon and sulphur contents of samples (LECO, 2015).

Image pre-processing

The recorded NIR hyperspectral images needed pre-processing to improve the performance of the SIMPLISMA method and the classification of pixel spectra with correlation coefficients. The first pre-processing step that was applied was to convert the recorded data to relative reflections. This was performed with Corescan's in-house software by using a calibration of a white reference and a dark current. A white reference is a measurement of a material with almost 100% reflection over the 450 to 2500 nm spectral range. A dark current is a measurement that is performed when no light enters the sensor in order to record instrumental noise.

The second pre-processing step that was applied was to mask the image by removing the data of pixels that do not represent a sample. This was performed by manually selecting regions of interest on the image. Subsequently, the data of pixels that contain anomalies was removed. These anomalies are wavelength bands with reflections > 100% or < 0% that are caused by errors in the detection mechanism of the NIR-HI sensor. Figure 3 presents the 1400 nm wavelength band of the hyperspectral image after masking and removal of pixels with anomalies. The order in which samples are presented in this figure is equal to that of figure 2.

The third pre-processing step was to subdivide the spectral range of the NIR hyperspectral image into two regions. This was done because two different types of mineral absorptions take place on the spectral range that was recorded. At wavelengths ranging from 450 to 1330 nm the pixel spectra are dominated by charge transfer absorptions of the Fe-ion (Fe^{2+} and Fe^{3+}). These absorptions therefore allow determination of Fe-bearing mineralogy. This wavelength region will be referred to as the visible (VIS) region of the NIR spectra. At wavelengths ranging from 1330 to 2500 nm the pixel spectra are dominated

 ISBN: 978-1-926872-32-2

by absorptions that are produced by molecule bond vibrations. These absorptions allow determination of hydrothermal alteration mineralogy. This wavelength region will be referred to as the short wave infrared (SWIR) region of the NIR spectra.

Figure 2 - Photograph of the sample set

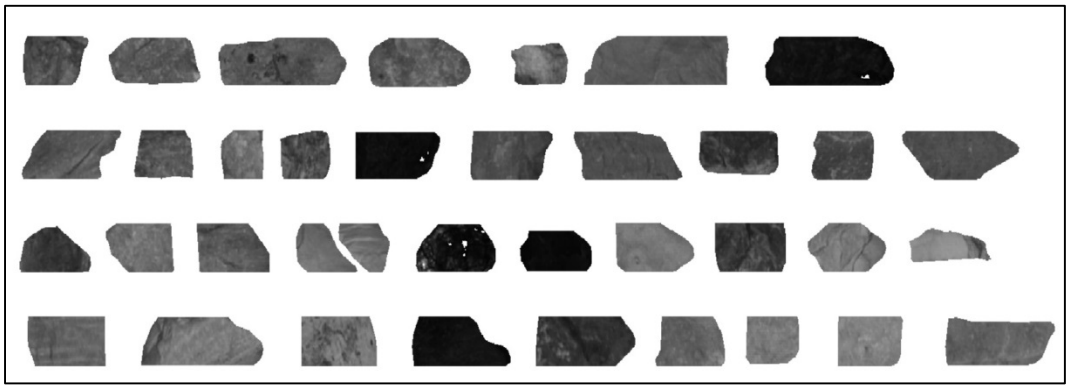

Figure 3 - Masked 1400 nm wavelength band of the measured NIR hyperspectral image

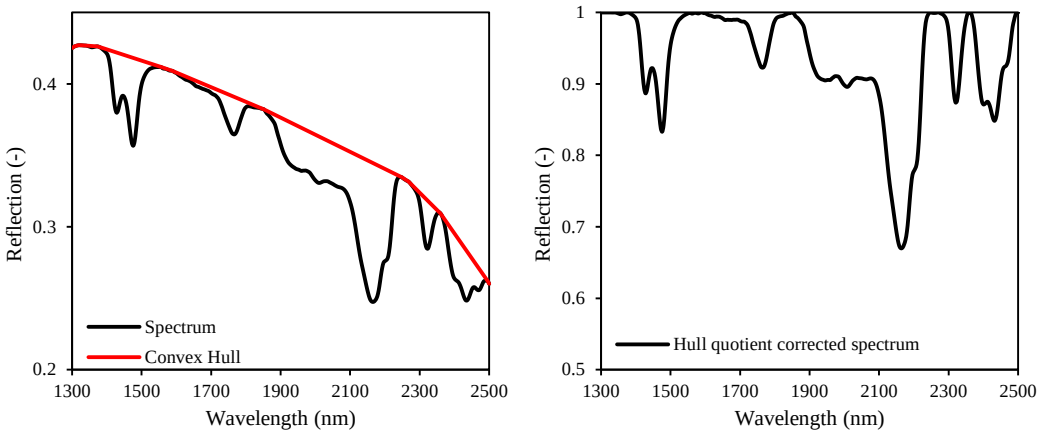

Figure 4 - Example of the hull quotient correction

 ISBN: 978-1-926872-32-2

The final pre-processing step that was applied was smoothing of the spectral data and correction of variations in the overall reflection of samples. Smoothing of the data reduces the noise that is present in the spectra. Smoothing was performed by using a Savitzky-Golay filter with a second order polynomial. Correcting variations in the overall reflection of samples was needed to remove absorption effects that are not indicative of mineralogy. These include light scattering, particle-size effects, surface roughness and detector artifacts (Amigo, 2010). Different methods for correcting the overall reflection were applied to the VIS and SWIR regions of the NIR spectra. The methods were chosen in order to provide the best correction for the type of mineral absorptions that takes place in these spectral regions. The VIS spectra were corrected by converting the data to standard normal variates, i.e. setting the mean and standard deviation of the VIS spectra to 0 and 1 respectively. The SWIR spectra were corrected by using the hull quotient removal. In this type of correction the convex hull of the spectrum is calculated which represents the shape of the spectrum without the absorption features. Each wavelength band of the spectrum is divided by the convex hull to produce the corrected spectrum. The hull quotient removal is illustrated in figure 4.

RESULTS

Mineralogy determined from the NIR hyperspectral images

Figure 5 presents an overview of measured NIR spectra of all the different minerals that were determined on the samples with NIR-HI. The minerals determined from the VIS region of the NIR spectra are presented separately of those from the SWIR region. Almost all spectra in figure 5 match those of single minerals (AusSpec, 2008; Clark, et al., 2007). Only the SWIR spectrum of dickite is mixed with other minerals. The absorption features that led to identification of dickite from this spectrum are those that occur at 1380, 1415, 2175 and 2205 nm. The broad feature that occurs at 1920 nm is produced by water and the small feature at 1476 nm by alunite.

The spectrum of water that is presented in figure 5 is likely produced by fluid inclusions in quartz. The occurrence of quartz with fluid inclusions is common at epithermal deposits (Simmons, White, & John, 2005). For samples on which all the pixel spectra represented that of water, also quartz contents > 90% were determined by XRD. It was made sure that all samples were dry while taking the measurements.

The spectrum of hematite / goethite that is presented in figure 5 is actually more representative for goethite than for hematite. However, it was not always possible to distinguish between hematite and goethite from the VIS region of the pixel spectra. This is because these minerals often occur together and their absorption features overlap. For this reason, hematite and goethite were classified as one group to produce mineral distribution maps from the NIR hyperspectral images.

The SWIR region of the pixel spectra often contains absorptions by 2 or 3 different minerals. In total, 13 different combinations of NIR active mineral assemblages were classified to produce mineral distribution maps from the SWIR region of the NIR hyperspectral images. From the VIS region of the pixel spectra only a dominant mineralogy was classified. A fraction of the pixel spectra also contained no characteristic absorptions on the VIS region at all, indicating an absence of Fe-bearing minerals.

Apart from the spectra that are presented in figure 5, also pixel spectra with a very low reflection over the entire VIS and SWIR spectral ranges were measured. It resulted that these spectra are representative for the carbonaceous ore materials. The low reflection of carbonaceous samples is also observed visually from their dark black colour.

For most of the samples XRD validated the occurrence of all minerals that were identified with NIR-HI. The only minerals that were not always validated are diaspore, alunite, dickite and hematite / goethite. Diaspore was validated on 7 out of 12 samples on which it was determined with NIR-HI. Alunite was not validated on any of the 4 samples on which it was determined with NIR-HI. However, alunite was determined by XRD on one other sample. On this sample no spectra representing alunite were found

 ISBN: 978-1-926872-32-2

among the pixels of the hyperspectral image. Dickite was identified on only 1 sample with NIR-HI and this was not validated by XRD. Dickite was also not determined by XRD on any other samples. Hematite / Goethite was validated on only 1 out of 18 samples on which it was determined with NIR-HI.

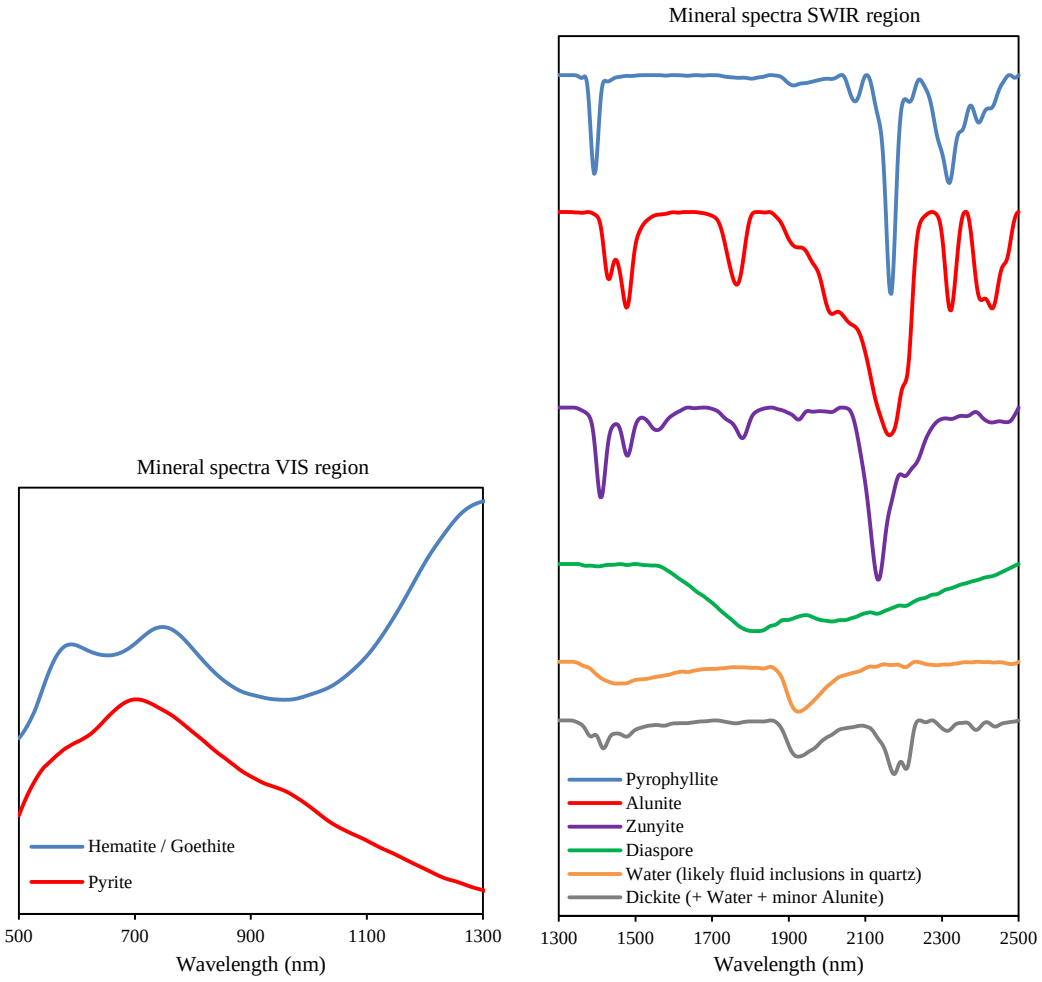

Figure 5 - Mineral spectra extracted from the measured NIR hyperspectral images

The fact that XRD did not always allow validation of the mineralogy identified with NIR-HI is likely caused by the way in which the samples are used in both techniques. XRD was performed on pulverized samples and the mineralogy determined by this technique therefore represents the whole volume of the sample. With NIR-HI however, the mineralogy is determined on only the outer surface of the sample. The samples used in the testwork are not homogeneous and are formed by breakage of rock formations that consist of many small veins and fractures. When the rocks break along these veins and fractures, the outer surfaces of the samples may have a different mineral composition than the entire sample volume. When small veins and fractures cross-cut the sample on the other hand, the sample volume may contain minerals that are not visible from the surface. Furthermore, both XRD and NIR-HI have a certain detection limit. It is therefore possible that minerals occurring in low concentrations were not detected. However, almost all minerals that were determined from the entire sample set with NIR-HI were also determined with XRD. This indicates that identification of mineralogy from the NIR hyperspectral images was correct. Only for dickite it is not certain that this mineral was correctly identified.

 ISBN: 978-1-926872-32-2

Image classification

Classification on C

The first step in the hyperspectral image classification was to classify spectra that represent carbonaceous ore material. The pixel spectra of carbonaceous materials have a very low reflection over the entire VIS and SWIR spectral ranges. This results in relatively low signal to noise ratios. Furthermore, these pixel spectra usually do not contain mineral absorption features. This has detrimental effects on the techniques applied for extracting the pure pixel spectra and the classification with correlation coefficients. It was therefore necessary to remove the pixels of carbonaceous ore material from the dataset. Figure 6 presents the 1400 nm wavelength band of the NIR hyperspectral image on which pixels with an average reflection < 10 % over the entire 450 to 2500 nm spectral range are assigned a red colour. The black rectangles in this figure indicate samples that have C contents > 0.50 %. All other samples have C contents < 0.50 %. It is clear from figure 6 that samples with relatively high C contents can be distinguished with NIR-HI. These samples were removed from the dataset for producing the mineral distribution maps.

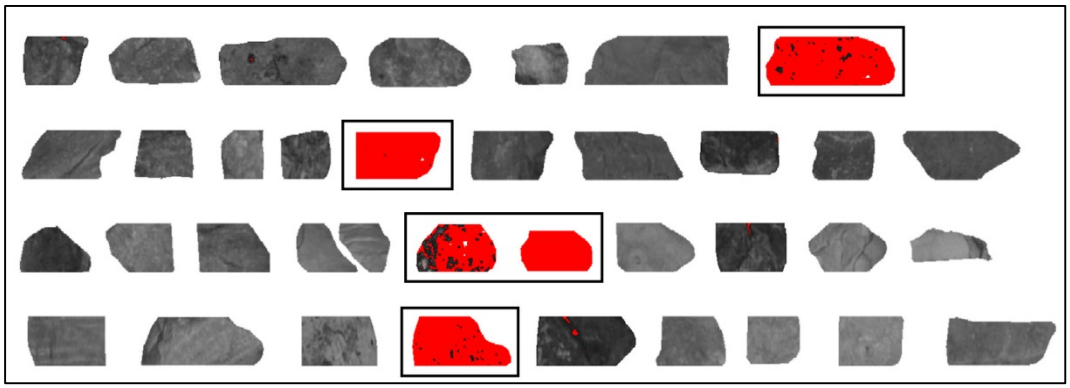

Figure 6 - 1400 nm wavelength band of the measured NIR hyperspectral image. Pixels with an average reflection < 10 % on the 450 – 2500 nm wavelength range are assigned a red colour. The black rectangles indicate carbonaceous ore samples.

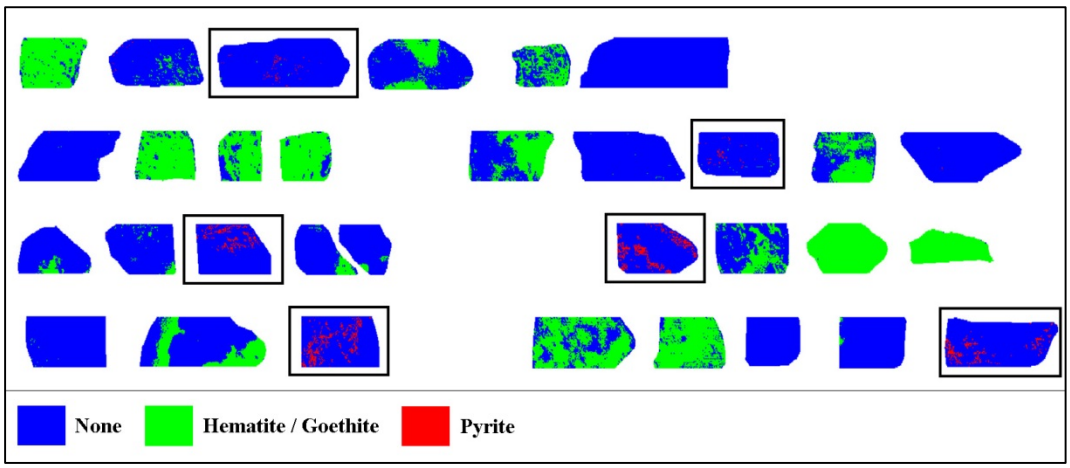

Figure 7 - Mineral distribution map of the VIS region of the NIR hyperspectral image. The black rectangles indicate samples on which pixel clusters of pyrite occur.

 ISBN: 978-1-926872-32-2

Classification on S

Figure 7 presents the mineral distribution map that was produced on VIS region of the NIR hyperspectral images. The black rectangles in this figure indicate samples on which clusters of pixels occur that are classified as pyrite. According to the XRD results, pyrite (FeS_2) is the only sulphide mineral that occurs in the samples. Table 1 presents the differences in S content if the samples with clusters of pyrite pixels in the mineral distribution map of figure 7 are distinguished from all other samples. This table shows that significant differences result between the average S content of both groups. Furthermore, the table shows that samples containing cluster of pyrite pixels have a minimum S content of 0.57 %. It therefore results that NIR-HI can be used to distinguish ore particles with relatively high S contents. However, samples could not be distinguished on a certain S content cut-off. Table 1 shows that there is still overlap between the distributions of the S content of both groups.

Table 1 - Results of classification on pyrite pixel clusters

	Total	Samples with pyrite clusters in figure 7	Other samples
Fraction of samples (%)	100	19.4	80.6
S (%) minimum	0.00	0.57	0.00
S (%) maximum	9.48	9.48	2.22
S (%) average	0.76	2.80	0.27

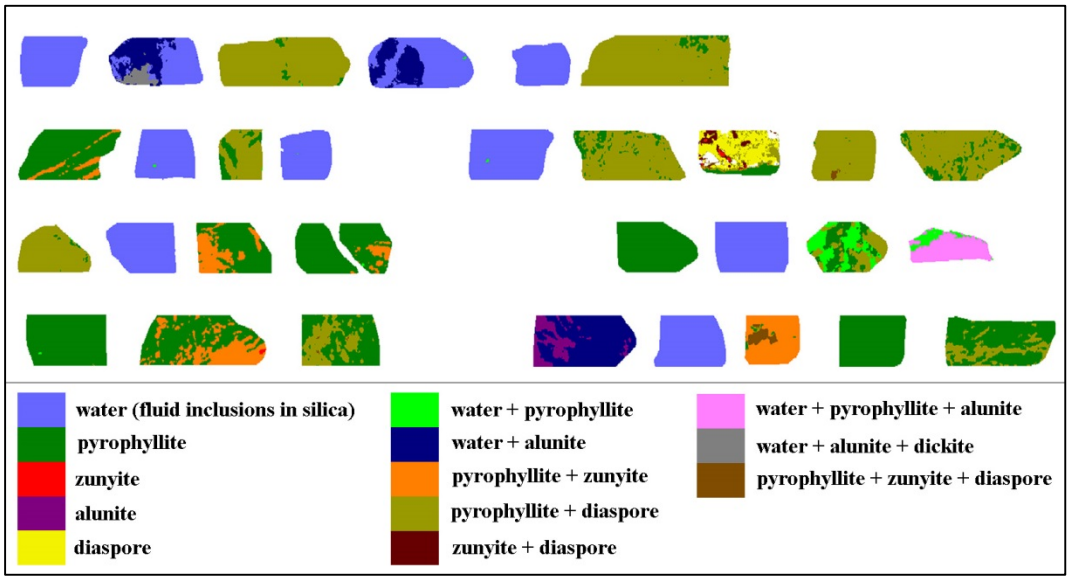

Figure 8 - Mineral distribution map of the SWIR region of the NIR hyperspectral image.

Classification on Au & Ag

Figure 8 presents the mineral distribution map that was produced on SWIR region of the NIR hyperspectral images. This map shows that the NIR active mineralogy of almost all samples is dominated by either pyrophyllite or water (fluid inclusions in quartz). Only one sample occurs on which diaspore is

 ISBN: 978-1-926872-32-2

the most abundant NIR active mineral. Alunite and dickite only occur on samples where water spectra dominate. Diaspore and zunyite only occur when pyrophyllite is present. Mixed pixel spectra of water and pyrophyllite are also observed on the samples, but their occurrence is usually very minor. On only 2 samples this mixture is present in a relatively large amount (figure 8: 3rd row, first 2 samples from the right).

By comparing the mineral distribution map of figure 8 with the Au and Ag grades of samples, it resulted that samples dominated by pyrophyllite have lower Au and Ag grades than those dominated by water. It also resulted that samples containing pyrophyllite and zunyite have higher Au grades than samples that contain only pyrophyllite or samples that contain pyrophyllite and diaspore. Based on these results, the mineral distribution map of figure 8 was modified to produce the waste discrimination map that is presented in figure 9. The red pixels on the map in figure 9 represent spectra of pyrophyllite and pyrophyllite + diaspore that are indicators of low Au and Ag grades. The green pixels represent spectra of zunyite and pyrophyllite + zunyite that indicate that a sample can have a higher Au grade. All other pixels in figure 9 show the 1400 nm wavelength band of the hyperspectral image and have no influence the identification of waste samples. Table 2 presents the results when samples containing red pixels and no green pixels in the waste discrimination map of figure 9 are distinguished from the rest of the sample set. These samples are also indicated by the black rectangles in figure 9.

Table 2 shows that significant differences result between the average Au and Ag grades when samples are distinguished by using the waste discrimination map of figure 9. Furthermore, the table shows that the samples that can be distinguished contain no Ag and have a maximum Au grade of only 0.17 ppm. It therefore results that NIR-HI can be used to distinguish ore particles with relatively low Au and Ag grades. However, not all samples below a certain Au grade cut-off could be identified with NIR-HI. Table 2 shows that the distribution of Au grades of both groups completely overlap. If the results in table 2 can be reproduced with sensor based sorting equipment though, this is not problematic. Since sensor based sorting is generally cheaper than the conventional ore processing methods (Salter & Wyatt, 1991; Sivamohan & Forssberg, 1991; Wotruba & Riedel, 2005), removal of only a fraction of the low grade ore material could already provide economic benefits. That is, if the value of the amount of Au and Ag that are lost by discarding ore material through sensor based sorting do not exceed the difference in costs between sensor based sorting and conventional ore processing. However, no economic analysis of sensor based sorting was performed on the results in table 2. The results do show that there is great potential in using NIR-HI for sensor based sorting of epithermal Au-Ag ore.

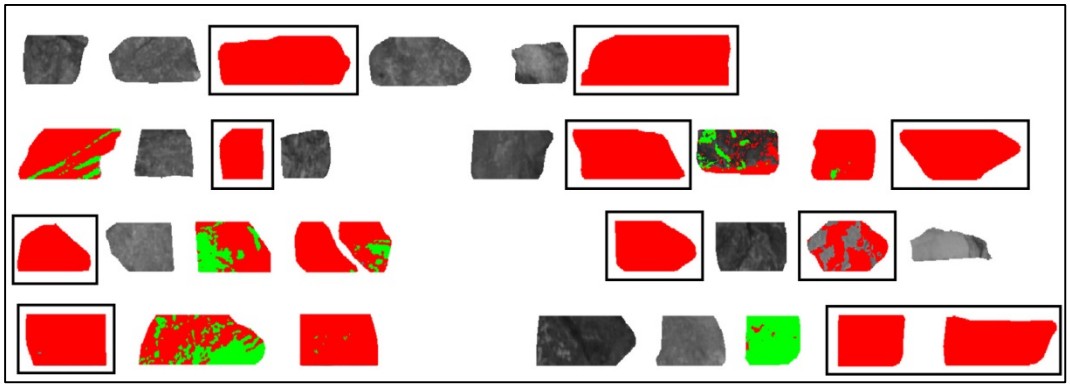

Figure 9 - Waste discrimination map. Red pixels indicate waste and represent spectra of pyrophyllite and pyrophyllite + diaspore. Green pixels indicate a sample is not waste regardless of any red pixels. Spectra of green pixels represent zunyite and pyrophyllite + zunyite. The black rectangles indicate samples on which only red pixels occur.

 ISBN: 978-1-926872-32-2

Table 2 - Results of classification with the waste discrimination map of figure 9

	Total	Samples with red pixels and no green pixels in figure 9	Other samples
Fraction of samples (%)	100	35.5	64.5
Au (ppm) minimum	0.02	0.02	0.02
Au (ppm) maximum	3.59	0.17	3.59
Au (ppm) average	0.26	0.08	0.36
Ag (ppm) minimum	0.00	0.00	0.00
Ag (ppm) maximum	14.90	0.00	14.90
Ag (ppm) average	1.59	0.00	2.47

REPRESENTATIVITY OF THE RESULTS

A limitation of the results presented here is the representativity of the used sample set. This is mainly directed at the results on distinguishing samples with low Au and Ag grades. These results are based on an indirect relationship to certain alteration mineral assemblages, while it is unknown if this relationship persists throughout the entire ore deposit. In order to validate these results, research is needed on a sample set that covers all geological and mineralogical variability of the deposit. This research is currently ongoing at Delft University of Technology in The Netherlands.

CONCLUSIONS

The following conclusions were drawn from the testwork:

- The average reflection over the entire 450 – 2500 nm spectral range can be used to distinguish samples with relatively high C contents.
- It is possible to use NIR-HI to distinguish ore samples with high S contents. This is based on detecting pyrite from the VIS region of the pixel spectra (350 – 1300 nm).
- It is possible to use NIR-HI to distinguish ore samples with low Au and Ag grades. This is based on specific alteration mineral assemblages detectable from the SWIR region of the pixel spectra (1300 – 2500 nm).
- More research is needed to validate the results on a sample set that is more representative for the geological and mineralogical variability of the entire deposit.

ACKNOWLEDGEMENTS

The authors would like to thank Barrick Gold for providing test samples and funding for this research.

 ISBN: 978-1-926872-32-2

REFERENCES

Amigo, J. (2010). Practical issues of hyperspectral imaging analysis of solid dosage forms. *Analytical and Bioanalytical Chemistry, 398*, 93-109.

AusSpec. (2008). *G-MEX Spectral interpretation field manual* (3 ed.). AusSpec International ltd.

Bergmann, J. (2011). Sensor based sorting. *Industrial Minerals, July*.

Buxton, M., & Benndorf, J. (2013a). The use of sensor derived data in optimization along the mine-value-chain. In s.n. (Ed.), *International congress of the ISM* (pp. 324-336). Clausthal-Zellerfeld: Papierflieger.

Buxton, M., & Benndorf, J. (2013b). The use of sensor derived data in real time mine optimization: A preliminary overview and assessment of techno-economic significance. In s.n. (Ed.), *Proceedings of the 2013 SME Annual Meeting* (pp. 215-219). SME.

Clark, R. (1999). Spectroscopy of rocks and minerals and principles of spectroscopy. In A. Rencz (Ed.), *Manual of remote sensing, remote sensing for the earth sciences, vol. 3* (pp. 3-58). New York: John Wiley and sons.

Clark, R., Swayze, G., Wise, R., Livo, E., Hoefen, T., Kokaly, R., & Sutley, S. (2007). *USGS spectral library splib06a: U.S. Geological Survey, Digital Data Series 321*. Retrieved May 2014, from http://speclab.cr.usgs.gov/spectral-lib.html

Dalm, M., Buxton, M., van Ruitenbeek, J., & Voncken, J. (2014). Application of near-infrared spectroscopy to sensor based sorting of a porphyry copper ore. *Minerals Engineering, 58*, 7-16.

Harbeck, H., & Kroog, H. (2008). New developments in sensor based sorting. *Aufbereitungstechnik, 49*(5), 4-11.

Hunt, G. (1977). Spectral signatures of particulate minerals in the visible and near infrared. *Geophysics, 42*(3), 501-513.

LECO. (2015). *LECO Carbon/Sulphur analyzers*. Retrieved 2015, from http://www.leco.com/products/analytical-sciences/carbon-sulfur-analyzers

Pirajno, F. (1992). *Hydrothermal mineral deposits, principles and fundamental concepts for the exploration geologist* (1st ed.). Berlin: Springer-Verlag.

Salter, J., & Wyatt, N. (1991). Sorting in the minerals industry: past, present and future. *Minerals Engineering, 4*, 779- 796.

Sillitoe, R. (1993). Epithermal models: genetic types, geometrical controls and shallow features. In R. Kirkham, W. Sinclair, R. Thorpe, & J. Duke (Eds.), *Mineral deposit modelling* (pp. 403-417). Geological Association of Canada, special paper 40.

Simmons, S., White, N., & John, D. (2005). Geological characteristics of epithermal precious and base metal deposits. *Economic Geology, 100th anniversary volume*, 485-522.

Sivamohan, R., & Forssberg, E. (1991). Electronic sorting and other preconcentration methods. *Minerals Engineering, 4*, 797-814.

Thompson, A., Hauff, P., & Robitaille, A. (1999). Alteration mapping in exploration: application of short-wave infrared (SWIR) spectroscopy. *Society of Economic Geologists Newsletter, 39*, 15-27.

White, N., & Hedenquist, J. (1995). Epithermal gold deposits: styles, characteristics and exploration. *Society of Economic Geologists Newsletter, 23*, 8-13.

Windig, W., & Guilment, J. (1991). Interactive self-modelling mixture analysis. *Analytical chemistry, 63*, 1425-1432.

Wotruba, H., & Riedel, F. (2005). Ore preconcentration with sensor based sorting. *Aufbereitungs technik, 46*(5), 4-13.